ECCOMAS Congress 2016
VII European Congress on Computational Methods in Applied Sciences and Engineering
M. Papadrakakis, V. Papadopoulos, G. Stefanou, V. Plevris (eds.)
Crete Island, Greece, 5–10 June 2016

NUMERICAL INVESTIGATION OF METASTABLE CONDENSING FLOWS WITH AN IMPLICIT UPWIND METHOD

L. Azzini, T.P. van der Stelt, M. Pini

Propulsion & Power group
Faculty of Aerospace engineering
Delft University of Technology
Kluyverweg, 1, Delft, Netherlands
contact e-mail: m.pini@tudelft.nl

Keywords: Two-phase flows, method of moments, nozzle expansion, metastable condensation, upwind flux

Abstract.

This work proposes and assesses two numerical models for solving high-speed condensing flows in metastable conditions. Each model involves a set of governing equations (mass, momentum, and energy) for the mixture or the continuum phase, i.e. the vapor, and two additional transport equations to characterize the dispersed phase. Such relations are formulated through the so-called method of moments that allows to represent the wetness fraction and the number of droplets of the liquid.

The transport relations are discretized in space by means of a new coupled up-wind scheme. A segregated implicit time integration strategy is exploited to hasten the convergence of the full system to steady-state. The performance and accuracy of both models are thoroughly investigated on a reference quasi-1D problem and confronted against experimental data and more advanced two-phase flow models.

Results show that experimental observations are adequately predicted, especially concerning the droplets dimension. It is additionally inferred that the new upwind flux is beneficial to improve robustness of the underlying numerical methods. Finally, it is demonstrated that the continuum phase model outperforms the mixture one in terms of numerical stability and computational cost, thereby making it very promising for the extension to multi-dimensional problems.

NOMENCLATURE

Acronyms	
EoS	Equation of State
ORC	Organic Rankine cycle
GDE	General Dynamic Equation

Symbols	
A	Numerical flux jacobian
$a1$	A matrix component
$a2$	$\|A\|$ matrix component
A_c	Cross sectional area
$b1$	A matrix component
$b2$	$\|A\|$ matrix component
$c1$	A matrix component
$c2$	$\|A\|$ matrix component
e	Internal energy
F	Numerical flux
f	Distribution function
G	Growth rate
h	Enthalpy
J	Nucleation rate
L_{eig}	Left eigenvectors matrix
M	Mach number
m	Mass
N	Droplet number per unit total mass
P	Pressure
Q	Source terms vector
R	Droplet radius
R_{eig}	Right eigenvectors matrix
S	Source term (mass balance)
T	Temperature
t	Time
U	Solution vector
V	Generic vector (residual jacobian)
v	Velocity
x	Space coordinate
Y	Liquid mass fraction

Greek letters	
α	Steam volume fraction
β	Empirical parameter (in J)
γ	Heat capacity ratio
Λ	Eigenvalues matrix
μ_j	Moment of order -j
ρ	Density

Subscripts	
*	Critical, correspondent to the Gibbs free energy maximum
0	Total property
average	Average properties on the domain (integral approximation)
c	Continuum phase
d	Dispersed phase
inlet	Domain inlet
m	Mixture
outlet	Domain outlet

1 INTRODUCTION

Metastable condensation of transonic and supersonic flows is subject of abundant numerical and experimental research. The accurate characterization of homogeneous condensation, which occurs when liquid particles (nuclei) can durably form in a supersaturated high-speed vapor, is extremely relevant in a variety of industrial processes, whereby the release of latent heat produces unwanted fluid-dynamic penalties. Typical examples are homogeneous condensation in low-pressure steam turbines [1] or in converging-diverging nozzles [2].

The numerical computation of condensing flows can be approached in three different ways [3] commonly classified in i) Eulerian-Lagrangian (EL) methods, ii) Eulerian-Eulerian (EE) methods, and iii) method of moments (MM). The key difference among them lies in the treatment of the additional transport equations used to describe the second (dispersed) phase. Notably, the EL and EE approaches model the entire spectrum of droplet sizes, while the MM accounts only for the low-order statistical moments of the size distribution.

A first comparison amongst the three models was performed in [3]. The study pointed out that the EL method features the highest accuracy at the expense of high computational cost. Moreover, the extension to unsteady simulations and flows characterised by slip between phases is particularly challenging. The full EE method has a similar accuracy compared to EL. However, it is affected by severe numerical instabilities that may compromise the convergence rate. Results showed that the cost of simulations with the EE was 50% more demanding than with the EL.

The MM, originally introduced by Hill [4] and increasingly adopted in many research studies [5, 6, 7], exhibited substantial computational efficiency gain with respect to EL and EE methods, thus is deemed the most suitable model for multi-dimensional calculations in engineering applications. However, the accuracy obtained may be considerably lower, especially regarding the droplets dimension. [3] reported a discrepancy of about 20% on the average droplets radius compared to experimental data.

In the context of MM, two formulations can be devised to describe the motion of the two-phase mixture. The former, referred to as mixture formulation [8], expresses the mass, momentum, and energy balance in terms of mixture properties, whereas the latter, referred to as continuum phase formulation, specifies the conservation laws in terms of vapor phase. For this last case, no examples are found in the literature, and this work refers to the framework devised in [9] for the EE method.

The aim of this work is to compare the two formulations in order to establish an efficient numerical framework for the resolution of multi-dimensional condensing flows. To this purpose, a quasi 1-D model is employed. The transport equations are discretized in space by a novel upwind scheme while the whole system of conservation laws is integrated in time using an implicit method to enhance the numerical stability as well as the convergence to steady-state. The results are carried out on a widely popular nozzle test case in which non-equilibrium condensation takes place.

The paper is structured as follows: the first section describes the governing equations and the necessary closure relations. The second section reports the numerical resolution adopted. Finally, the last section reports the validation of the models and debates the results of the MM against reference solutions obtained with the EL and the EE.

2 GOVERNING EQUATIONS

This work considers quasi 1-D condensing flows. In principle, eight governing equations are needed to obtain the averaged properties of the liquid and vapor phase, namely their thermodynamic states, the velocities, the liquid mass fraction and the droplet radius.

For condensing flows with limited liquid mass fractions, the following assumptions proved to be adequate: i) the liquid and vapor are in mechanical equilibrium, ii) no slip between the two phases, and iii) the temperature of the dispersed phase is determined through a capillarity model. As a result, three conservation laws supplemented by two transport equations for the dispersed phase properties are sufficient to characterize the mixture.

2.1 Conservation laws

The mass, momentum, and energy balance for the continuum phase are written as

$$\frac{\partial \rho_c}{\partial t} + \frac{\partial \left(\rho_c v_c\right)}{\partial x} = S_c - \rho_c v_c \frac{\partial A_\mathrm{c}}{\partial x}\frac{1}{A_\mathrm{c}}, \tag{1}$$

$$\frac{\partial \rho_c v_c}{\partial t} + \frac{\partial \left(\rho_c v_c^2 + p_c\right)}{\partial x} = S_c v_c - \rho_c v_c^2 \frac{\partial A_\mathrm{c}}{\partial x}\frac{1}{A_\mathrm{c}}, \tag{2}$$

$$\frac{\partial (\rho_c e_{0,c})}{\partial t} + \frac{\partial \left(\rho_c h_{0,c}\right)}{\partial x} = S_c h_{0,d} - \rho_c h_{0,c} \frac{\partial A_\mathrm{c}}{\partial x}\frac{1}{A_\mathrm{c}}, \tag{3}$$

where ρ_c is the phase density, v_c the velocity, P_c the pressure, $e_{o,c}$ the total internal energy, $h_{o,c}$ the total enthalpy, A_c is the cross sectional area and S_c is the source term accounting for mass exchange through the liquid-vapor interface, defined as

$$S_c = -\rho_m \frac{3Y}{R}\frac{\partial R}{\partial t}, \tag{4}$$

in which R is the averaged droplet radius and Y is the liquid mass fraction. The mixture equations can be retrieved by substituting in eq.(1) the mixture properties and neglecting S_c. For the sake of conciseness, mixture and the continuum phase approaches are referred to as model (a) and (b), respectively, hereafter.

Important differences arise between the two models: model (b) may suffer from more severe stiffness due to condensation source terms. On the contrary, in model (a) the thermodynamic non-equilibrium of the vapor phase renders the computation of the mixture properties iterative [8]. This procedure entails an extra computational burden and may affect the solver robustness. Eventually, note that the validity of model (b) is restricted to vapors containing negligible liquid volume fractions [9].

2.2 Method of Moments

As aforementioned, the method of moments replaces the full droplet size distribution with its low-order statistical moments. The generic moment of order -j is defined as

$$\mu_j = \int_0^\infty R^j f dr, \tag{5}$$

where f is the distribution function, i.e. the radial derivative of the droplet number density, such that the total number of droplets N is equal to

$$N = \int_0^\infty f dr. \tag{6}$$

As described in [5], the conservation law for each moment stems from the GDE (General Dynamic Equation) and eq.(5), obtaining

$$\frac{\partial}{\partial t}(\rho_m \mu_j) + \frac{\partial}{\partial x}(\rho_m \mu_j v_m) = j \cdot \int_0^\infty \rho_m R^{j-1} G f dr + \rho_m J(R_*) R_*^j, \tag{7}$$

where G is the growth rate, R_* the critical radius, and J the nucleation rate.

These equations are usually solved through the method proposed in [4]. Nevertheless, though the model well correlates the experimental data for the continuum phase, as reported in [3], the method involves the resolution of four equations instead of the two theoretically required. Moreover, G can be only expressed as linear combination of R in the form

$$G = k_1 R + k_2, \tag{8}$$

where k_1 and k_2 are two parameters depending on the thermodynamic properties of the two phases. As outlined in [3],[7], the discrepancy between the experimental and numerical droplet averaged radius is larger than 20%.

For these reasons, this work adopts a 2-equations method. Thus, the transport equations for the moments of order -0 and -3 are finally written as

$$\frac{\partial}{\partial t}(\rho_m \mu_0) + \frac{\partial}{\partial x}(\rho_m \mu_0 v_m) + \rho_m \mu_0 v_m \frac{\partial A_c}{\partial x}\frac{1}{A_c} = \rho_m J(R_*), \tag{9}$$

$$\frac{\partial}{\partial t}(\rho_m \mu_3) + \frac{\partial}{\partial x}(\rho_m \mu_3 v_m) + \rho_m \mu_3 v_m \frac{\partial A_c}{\partial x}\frac{1}{A_c} = \rho_m J(R_*) R_*^3 + 3\rho_m R^2 G N, \tag{10}$$

where μ_0 and μ_3 are

$$\mu_0 = \int_0^\infty f dr = N, \tag{11}$$

$$\mu_3 = \int_0^\infty R^3 f dr = R^3 \int_0^\infty f dr = N R^3. \tag{12}$$

The remaining terms in eq. (9) and(10), namely the growth rate G, the nucleation rate J, the critical radius R_*, are taken from [7].

2.3 Thermophysical model

The thermodynamic model used for the continuum phase is the polytropic Van der Waals EoS (Equation of State), that allows to account for metastabilities in the two-phase region. The enthalpy as well as the saturation temperature and pressure are taken from [11], while the density and the capillarity model are as in [9]. Finally, the surface tension is given by [12], whereas viscosity and thermal conductivity are determined through the Chung's model [13].

The thermodynamic properties for the mixture can be retrieved following the procedure in [8] by using the quasi-Newton algorithm. Furthermore, the speed of sound of the mixture is estimated through the expression

$$c_m = \left[\left(1 - \frac{\rho_m}{\rho_d} Y\right) \frac{1}{c_c^2} + \left(\frac{\rho_m}{\rho_d} Y\right) \frac{1}{c_d^2} \right]^{-\frac{1}{2}}. \tag{13}$$

Appendix A shows the procedure to obtain such relation.

3 NUMERICAL METHOD

The balance equations for either mixture or continuum phase are discretized using a cell-centered finite volume scheme of first order of accuracy [10]. The source terms are directly incorporated in the numerical flux without special treatment. On the contrary, the transport equations are discretized by using an upwind scheme specifically conceived in this study, which is further detailed in the following. The full set of governing equations is advanced in time by an implicit, segregated strategy. More precisely, at each iteration the mass, momentum, and energy equations are solved assuming frozen droplet properties.

3.1 Upwind scheme for transport equations

As can be observed, the last term of eq.(10) is a function of the radius R of the dispersed phase. Since R is in turn a combination of μ_0 and μ_3 through eq.(12) it can be readily incorporated in the left hand-side of eq.(10) by a simple algebraic manipulation as

$$\frac{\partial}{\partial t}(\rho_m \mu_3) + \frac{\partial}{\partial x}(\rho_m \mu_3 v_m) + \frac{\rho_m \mu_3 v_m}{A_c}\frac{\partial A_c}{\partial x} = \rho_m J(R_*) R_*^3 + \frac{\partial}{\partial x}\left(\int 3\rho_m R^2 G N dx\right). \quad (14)$$

The last integral is approximated as

$$\int 3 \cdot \rho_m R^2 G N dx = 3\left(\rho_m R^2 G N\right)_{average} \cdot (x - x_{inlet}) = \sum_{i=0}^{x_{out}} 3\left(\rho_m R^2 G N \frac{\Delta x}{x_{outlet} - x_{inlet}}\right)_i \cdot (x - x_{inlet}), \quad (15)$$

where x_{inlet} and x_{outlet} are the inlet and outlet abscissas of the domain. Concisely, the 2 transport equations can be written as

$$\frac{\partial}{\partial t}U + \frac{\partial}{\partial x}F = Q, \quad (16)$$

where

$$U = \begin{bmatrix} \rho_m \mu_0 \\ \rho_m \mu_3 \end{bmatrix} = \begin{bmatrix} \rho_m N \\ \rho_m N R^3 \end{bmatrix}, \quad (17)$$

$$Q = \begin{bmatrix} \rho_m J(R_*) \\ \rho_m J(R_*) R_*^3 \end{bmatrix} - U \cdot v_m \frac{\partial A_c}{\partial x}\frac{1}{A_c}, \quad (18)$$

$$F = \begin{bmatrix} \rho_m \mu_0 v_m \\ \rho_m \mu_3 v_m - \sum_{i=0}^{x_{out}} 3\left(\left(\rho_m \mu_0\right)^{\frac{1}{3}} \left(\rho_m \mu_3\right)^{\frac{2}{3}} G \cdot \frac{\Delta x}{x_{outlet} - x_{inlet}}\right)_i \cdot (x - x_{inlet}) \end{bmatrix}. \quad (19)$$

The final up-wind flux is given by

$$F_{\frac{i+j}{2}} = \frac{F_i + F_j}{2} - |A|_{\frac{i+j}{2}} \frac{U_j - U_i}{2}, \quad (20)$$

in which the physical flux F is approximated for every cell -i as

$$\sum_{j=1}^{i} 3\left(\rho_m R^2 G N \cdot \frac{\Delta x}{x_{outlet} - x_{inlet}}\right)_j \quad (21)$$

Appendix B reports the spectral decomposition of A while Appendix C illustrates the derivation of the Jacobian.

4 VALIDATION AND ASSESSMENT OF THE NUMERICAL MODELS

In this section, the results of model (a) and (b) are compared with the experimental data reported in [3] and with existing numerical solutions obtained with more sophisticated methods. The selected test case is the well-established Moore nozzle A, which is representative of supersonic wet-steam flows occurring in turbine flow passages. The shape of the profile is reported in Appendix D. All the calculations are performed on a 1000-cells grid.

Fig.1 shows the dimensionless pressure distribution along the nozzle for the present models, the Hill's method [5] and experimental observations. No significant differences are found, especially prior and after the onset of condensation.

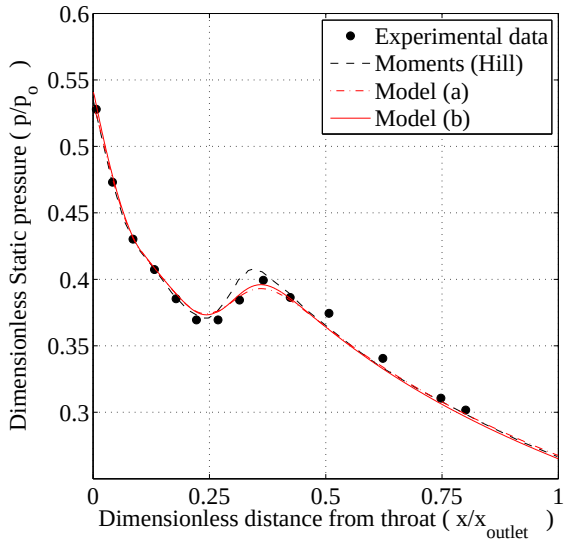

(a) Comparison bewtween model (a), model (b) and Hill's method

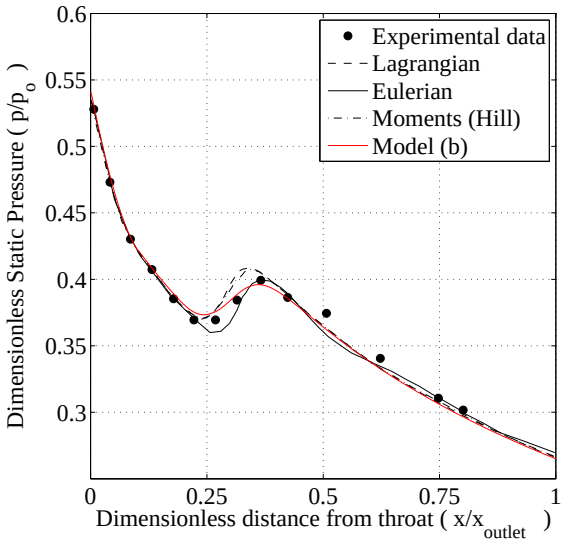

(b) Comparison between model (b) and the three approaches reported in [3]

Figure 1: Pressure distribution along the nozzle, $x_{throat} = 0$

The pressure trends of both liquid and vapor are depicted in the *T-s* chart of Fig.2. The same diagram shows the experimentally derived Wilson points, extrapolated from [14] for the considered pressure range. For the sake of clarity, the same curves are also displayed in the *P-v* plane of Fig.3. When the steam subcooling is close to 50K (from Fig.2) and the continuum phase reaches the Wilson point, condensation starts rapidly. The sudden release of latent heat leads to a considerable static temperature rise of the continuum phase which is quickly brought back to thermodynamic equilibrium. The amount of heat released is proportional to the nucleation rate, see Fig.4, which shows a steep peak from 0 to $2 \cdot 10^{21} kg^{-1}s^{-1}$ in a narrow portion of the nozzle close to the throat.

A more in-depth physical explanation of the condensation phenomenon can be figured out by inspecting Eq.(22), valid for ideal compressible channel flow with heat addition [15]

$$\frac{dP}{P} = \frac{\gamma M^2}{1 - M^2} \left(\frac{dA_c}{A_c} - \left(1 + \frac{\gamma - 1}{2} M^2 \right) \frac{dT_0}{T_0} \right), \tag{22}$$

in which M is the mach number, T_0 is the total temperature, and γ the specific heat ratio. In the early stage of condensation, the dominant term of Eq.(22) is the total temperature increase which causes a sudden static pressure rise, usually referred to as condensation shock wave.

The flow then departs from metastable conditions to reach thermodynamic equilibrium. As the condensation proceeds, the nucleation rate J falls down, therefore the release of latent heat and the total temperature variation reduce correspondingly. The flow motion is thus mainly governed by the area variation dA_c, which is positive for the given nozzle shape. Provided that the flow remains supersonic downstream of the shock, the expansion continues along the saturation line, as shown in both Fig.2 and 3.

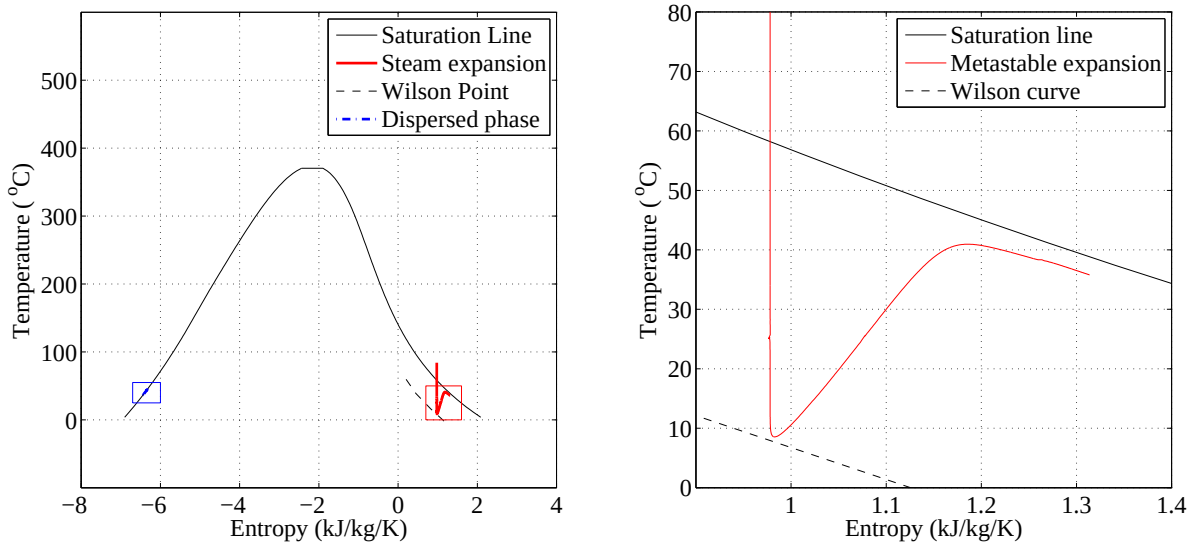

(a) Liquid and vapor thermodynamic conditions

(b) Detail of the vapor expansion

Figure 2: Liquid and vapor expansion reported in the *T-s* diagram for model (a)

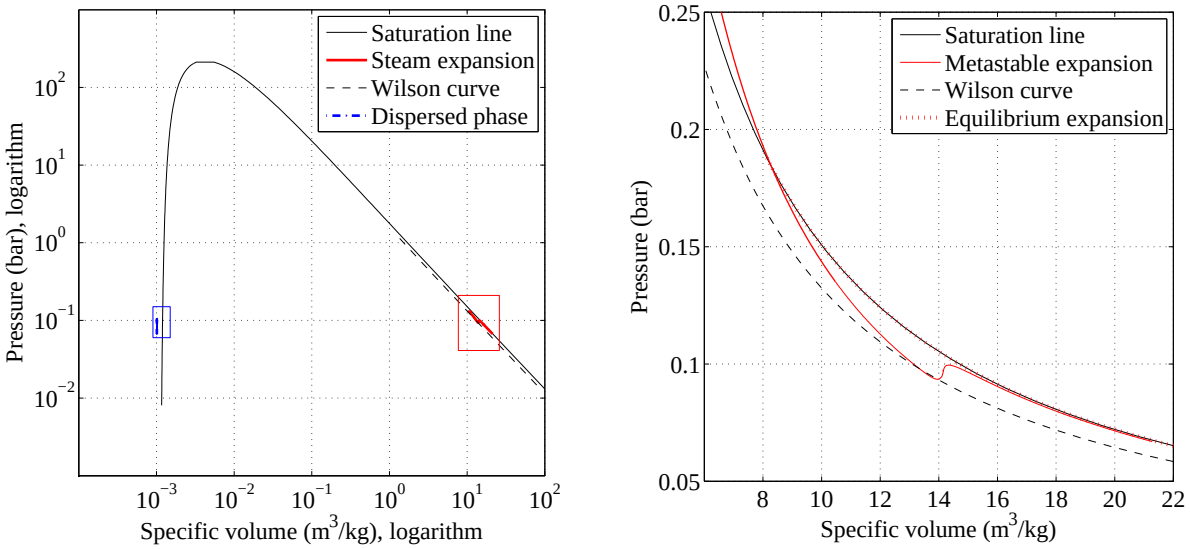

(a) Liquid and vapor thermodynamic conditions

(b) Detail of the vapor expansion

Figure 3: Liquid and vapor expansion reported in the *P-v* diagram for model (a)

As stated in [9], the liquid properties are barely dependent on the pressure in the specific thermodynamic range considered ($P < 0.25$ bar), see Fig.6. Furthermore, the temperature

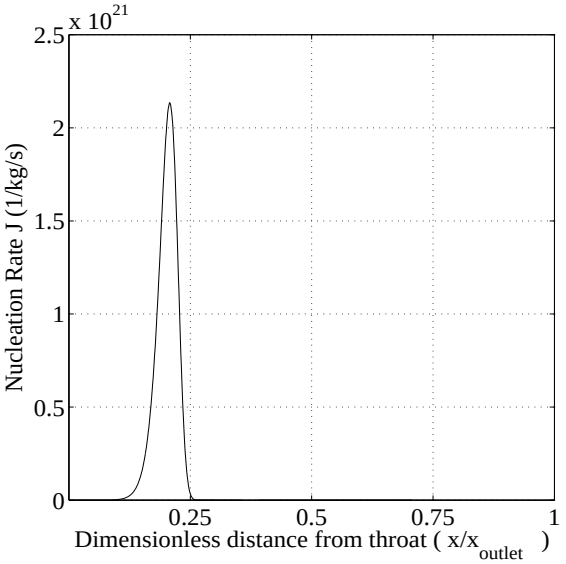

Figure 4: Nucleation rate along the nozzle, $x_{throat} = 0$

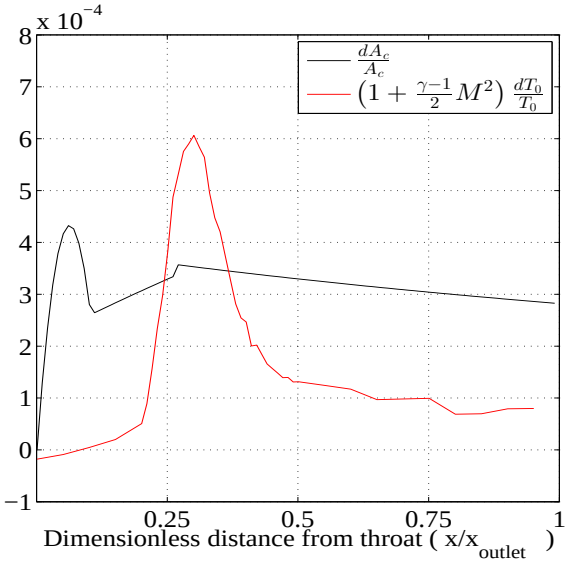

Figure 5: Main terms of eq.(22) along the nozzle, $x_{throat} = 0$

of the droplets T_d is few degrees higher than the vapor, according to the capillarity model. Therefore, it can be inferred that the dispersed phase expansion is located close to the saturation line, with a slight temperature difference with respect to the steam, as proved by fig.2 and 3.

Fig.7 shows that the major deviations between the various models are located in the condensation region. In particular, the Lagrangian and the Hill's method overestimate the pressure local maximum, whereas the Eulerian simulation predicts a higher degree of subcooling. Note however that the pressure slope between the two pressure extrema predicted by the three models is very similar, suggesting a fairly close value of nucleation rate. On the other hand, model (a) and (b) tend to underestimate the pressure bump. The reason can be partly attributed to the inaccuracy of the thermodynamic model adopted for the calculations. As anticipated, this work makes use of the polytropic Van der Waals EoS, arguably less accurate than the model devised in [3].

The droplet averaged radius is recognized as remarkably challenging to detect for all two-phase computational models. Fig.8 depicts the droplet radius along the nozzle. Unexpectedly, the results of model (a) and (b) are in good agreement with the experimental data, with an deviation of 5% (0.095μm diameter instead of 0.1μm nominal) for model (b) and much lower for model (a). Conversely, the discrepancy for the Hill's method has been found higher than 20% (with a diameter of 0.077μm) and even worse for the Eulerian approach, which features deviations larger than 30%.

A numerical study was conducted to assess the convergence rate of model (a) and (b). The benchmark is the so-called single phase simulation, where it is supposed the vapor expanding in the nozzle without inception of condensation. Despite this simulation has no physical meaning, it is commonly utilized as reference for examining the convergence properties of the various methods. The simulations were carried out by discretizing the nozzle with 400 cells and employing the Euler explicit integration scheme with CFL number equal to 1. Convergence was achieved after reducing the residuals of all equations by five orders of magnitude. Table 1 reports the final results. Notwithstanding comparable accuracy, model (a) is three times more demanding than model (b). The rationale of this difference has been found in the iterative

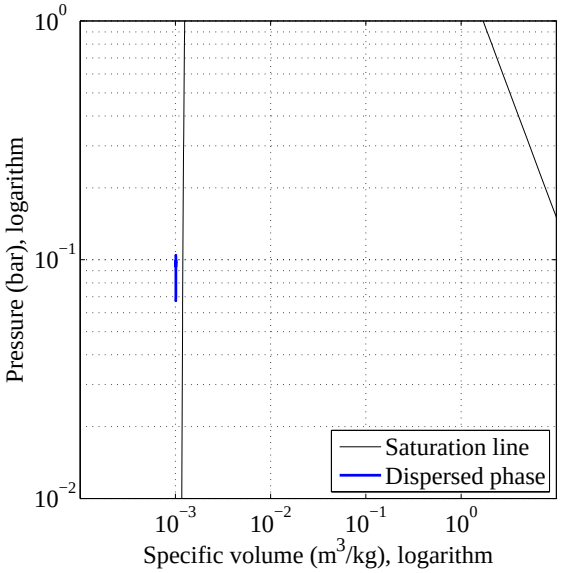

Figure 6: Detail of the liquid expansion from Fig. 3a, $x_{throat} = 0$

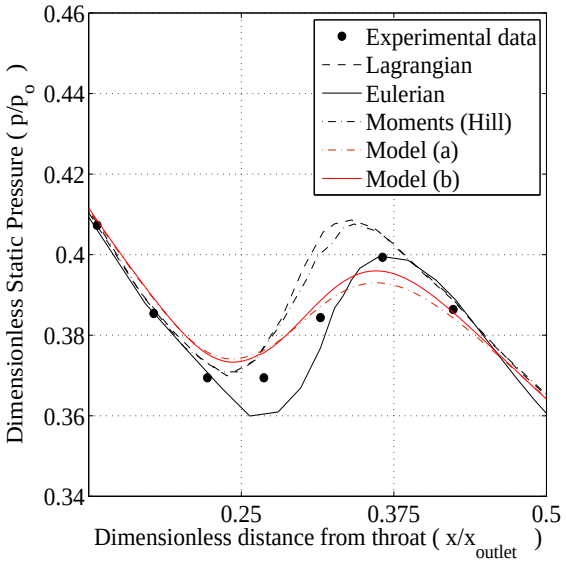

Figure 7: Detail of the pressure profile, comparison with [3], $x_{throat} = 0$

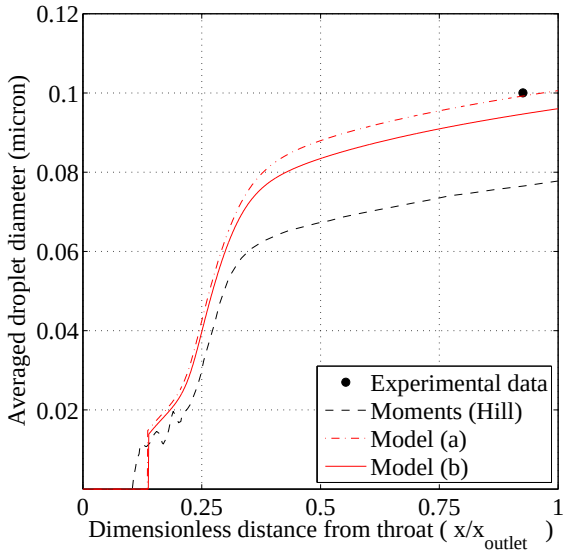

(a) Comparison between model (a), model (b) and Hill's method

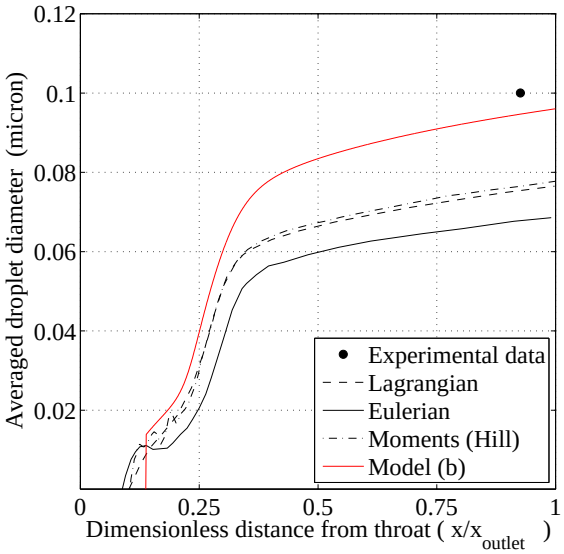

(b) Comparison between model (b) and the three approaches reported in [3]

Figure 8: Averaged droplet diameter along the nozzle, $x_{throat} = 0$

algorithm, i.e. quasi-Newton method, adopted for computing the mixture properties.

A final analysis was carried out to investigate the numerical stability of both models. Several simulations were run on a mesh of 400-cells with the implicit method for progressively increasing CFL numbers. Table 2 lists the obtained results in terms of maximum allowable CFL number.

As expected, the maximum time step for the two-phase flow systems is significantly lower than for the benchmark. This is mainly due to the stiffness introduced by the onset of condensation which occurs at much faster time scale than wave propagation in the flow. On the other

	Benchmark	Model (a)	Model (b)
Iterations	5024	4700	4823
Physical time (s)	14	79	25

Table 1: Simulation time required for the benchmark (single-phase), model (a) and model (b), explicit time integration, CFL=1

	Benchmark	Model (a)	Model (b)
Maximum CFL	102	28	46

Table 2: Maximum allowable CFL for the benchmark (single-phase), model (a) and model (b). The computations are performance with implicit time integration and constant CFL

hand, the comparison shows that model (a) allows for a maximum CFL that is nearly half of the one of model (b).

5 CONCLUSIONS

In this study, two flow models based on the method of moments for quasi-1D condensing flows were compared to more advanced approaches based on the lagrangian, the full eulerian, and the Hill's formulation. The governing equations were formulated in terms of mixture or vapor phase (alternatively called continuum phase) properties while the method of moments was used to characterize the liquid wetness fraction and droplets number. A novel upwind flux was proposed to solve for the additional transport equations. Implicit time integration was adopted to enhance convergence to steady-state.

Both models were tested on a reference nozzle case for which experimental data exist. The results showed that both models are capable to predict the pressure distribution along the nozzle with accuracy similar to that of the more sophisticated flow models. Remarkably, the computed diameter of the droplets resulted very close to the experimental evidences.

Lately, a numerical study was conducted to assess the computational cost as well as the numerical stability of the two models. It was inferred that the introduction of the up-wind flux for the moments relations provided high robustness to the underlying numerical method. However, the analysis revealed that the mixture model is approximately three times more demanding than continuum phase model if solved by adopting the same CFL number and up to six times less efficient for maximum CFL number warranting stability. The main motivation was found to be associated with the iterative procedure used to retrieve the mixture properties.

Envisaged steps forward to the current work will include i) the investigation of a more efficient iterative algorithm, ii) the coupling with more complex equations of state iii) the validation of the models against condensing steam flows at high-pressure and ii) the extension to multi-dimensions to be pursued in the framework of an existing open-source CFD solver.

REFERENCES

[1] J.B. Young, *Two-Dimensional, Non-Equilibrium, Wet-Steam Calculations for Nozzles and Turbine Cascades*, Journal of Turbomachinery 114, 569-579, 1992

[2] D.G. Elliot, E. Weinberg, *Acceleration of Liquids in Two-Phase Nozzles*, Technical report 32-987, National Aeronautics and Space Administration, 1968

[3] A.J. White, *A comparison of modelling methods for polydispersed wet-steam flow*, International journal for numerical methods in engineering 57, pp. 819834 (DOI: 10.1002/nme.705), 2003

[4] P.G. Hill, *Condensation of Water Vapour during Supersonic Expansion in Nozzles*, Journal of Fluid Mechanics, Vol. 25, part 3, pp. 593-620, 1966.

[5] F. Put, *Numerical Simulation of Condensation in Transonic Flows*, Thesis University of Twente, Enschede, 2003

[6] A.G. Gerber, A. Mousavi, *Application of quadrature method of moments to the polydispersed droplet spectrum in transonic steam flows with primary and secondary nucleation*, Applied Mathematical Modelling 31, pp. 15181533, 2007

[7] M. Giordano, S.J. Hercus, P. Cinnella, *Effects of modelling uncertainties in condensing wet-steam flows through supersonic nozzles*, V European Conference on Computational Fluid Dynamics ECCOMAS, Lisbon, Portugal,14-17 June 2010

[8] S. Dykas, W. Wróblewski, *Numerical modelling of steam condensing flow in low and high-pressure nozzles*, International Journal of Heat and Mass transfer 55, 6191-6199, 2012

[9] A.G. Gerber, M.J. Kermani, *A pressure based EulerianEulerian multi-phase model for non-equilibrium condensation in transonic steam flow*, International Journal of Heat and Mass Transfer 47, pp. 22172231, 2004

[10] R.J. LeVeque, *Numerical Methods for Conservation Laws*, Birkhliuser Verlag, Basel, Switzerland, 1992

[11] W. Wagner et al., *The IAPWS Industrial Formulation 1997 for the Thermodynamic Properties of Water and Steam*, ASME Journal of Engineering for Gas Turbines and Power 122, pp. 150182, 2000

[12] N.B. Vargaftik, B.N. Volkov, L.D. Voljak , *International Tables of the Surface Tension of Water*, Journal of chemical Physics Ref.Data12, 817, 1983

[13] B.E. Poling, J.M. Prausnitz, J.P. O'Connell , *The Properties of Gases and Liquids*, 5th edition, McGraw-Hill, 2001

[14] V.N. Gorbunov, Y.A. Ryzhov, U.G. Pirumov, *Non equilibrium Condensation in High-speed Gas Flows*, Gordon and Breach Science Publishers, 1989

[15] E.M. Greitzer, C.S. Tan, M.B. Graf, *Internal Flow, Concept and Applications*, Cambridge Engine Technology Series (No. 3), Cambridge University Press, 2004

A Thermodynamic derivatives for a mixture

The speed of sound is defined as

$$c_m = \left(\frac{\partial P}{\partial \rho_m}\right)_{s_m}^{\frac{1}{2}}. \tag{23}$$

The introduction of the continuum phase volume title α_c and the use of the derivation properties allow to rewrite eq.(23) as

$$c_m = \left(\frac{\partial \rho_m}{\partial P}\right)_{s_m}^{-\frac{1}{2}} = \left(\frac{\partial \left(\alpha_c \rho_c + (1-\alpha_c)\,\rho_d\right)}{\partial P}\right)_{s_m}^{-\frac{1}{2}}, \tag{24}$$

thus,

$$c_m = \left[\alpha_c \left(\frac{\partial \rho_c}{\partial P}\right)_{s_m} + (1-\alpha_c)\left(\frac{\partial \rho_d}{\partial P}\right)_{s_m} + (\rho_c - \rho_d)\left(\frac{\partial \alpha_c}{\partial P}\right)_{s_m}\right]^{-\frac{1}{2}}, \tag{25}$$

Two simplifications are made: i) the derivative of α_c is neglected and ii) the two derivatives at s_{mix} constant are approximated with the derivative of each phase, at constant s_c and s_d respectively. Furthermore, the volume title α_c is defined as

$$\alpha_c = \frac{V_c}{V_m} = 1 - \frac{V_d}{V_m} = 1 - \frac{\rho_m}{\rho_d} Y. \tag{26}$$

Therefore, the final expression for the speed of sound is

$$c_m = \left[\left(1 - \frac{\rho_m}{\rho_d} Y\right)\left(\frac{\partial \rho_c}{\partial P}\right)_{s_c} + \left(\frac{\rho_m}{\rho_d} Y\right)\left(\frac{\partial \rho_d}{\partial P}\right)_{s_d}\right]^{-\frac{1}{2}}, \tag{27}$$

thus,

$$c_m = \left[\left(1 - \frac{\rho_m}{\rho_d} Y\right)\frac{1}{c_c^2} + \left(\frac{\rho_m}{\rho_d} Y\right)\frac{1}{c_d^2}\right]^{-\frac{1}{2}}. \tag{28}$$

B Numerical flux derivatives for moments equations

B.1 Spectral decomposition

The flux jacobian A is determined from eq.(19) as

$$A = \left(\frac{\partial F}{\partial U}\right) = \begin{bmatrix} a_1 & 0 \\ b_1 & c_1 \end{bmatrix}, \tag{29}$$

in which

$$a_1 = \frac{\partial F(1)}{\partial U(1)} = v_m, \tag{30}$$

$$b_1 = \frac{\partial F(2)}{\partial U(1)} = -G\frac{x - x_{inlet}}{x_{outlet} - x_{inlet}} \Delta x \left(\rho_m \mu_0\right)^{-\frac{2}{3}} \left(\rho_m \mu_3\right)^{\frac{2}{3}}, \tag{31}$$

$$c_1 = \frac{\partial F(2)}{\partial U(2)} = -2G\frac{x - x_{inlet}}{x_{outlet} - x_{inlet}} \Delta x \left(\rho_m \mu_0\right)^{\frac{1}{3}} \left(\rho_m \mu_3\right)^{-\frac{1}{3}} + v_m. \tag{32}$$

As A is lower triangular, the eigenvalues matrix Λ is equal to

$$\Lambda = \begin{bmatrix} v_m & 0 \\ 0 & -2G\frac{x-x_{inlet}}{x_{outlet}-x_{inlet}}\Delta x\left(\rho_m\mu_0\right)^{\frac{1}{3}}\left(\rho_m\mu_3\right)^{-\frac{1}{3}} + v_m \end{bmatrix}. \tag{33}$$

The right and left eigenvector matrices R_{eig} and L_{eig} are

$$R_{eig} = \begin{bmatrix} \frac{v_m-c_1}{\sqrt{b_1^2+(v_m-c_1)^2}} & 0 \\ \frac{b_1}{\sqrt{b_1^2+(v_m-c_1)^2}} & 1 \end{bmatrix} \tag{34}$$

and

$$L_{eig} = \frac{1}{Det(R_{eig})}\begin{bmatrix} 1 & 0 \\ -\frac{b_1}{\sqrt{b_1^2+(v_m-c_1)^2}} & \frac{v_m-c_1}{\sqrt{b_1^2+(v_m-c_1)^2}} \end{bmatrix}, \tag{35}$$

where

$$Det(R_{eig}) = \left(\frac{v_m - c_1}{\sqrt{b_1^2 + (v_m - c_1)^2}}\right). \tag{36}$$

Therefore, $|A|$ is written as

$$|A| = R_{eig}|\Lambda|L_{eig} = \begin{bmatrix} a_2 & 0 \\ b_2 & c_2 \end{bmatrix} = \begin{bmatrix} v_m & 0 \\ \frac{b_1(v_m-|c_1|)}{v_m-c_1} & |c_1| \end{bmatrix}, \tag{37}$$

B.2 Boundary conditions

The number of boundary conditions that can be imposed is given by the eigenvalue analysis. From eq.(33), the first eigenvalue λ_1 is always positive. On the other hand, λ_2 may become negative. In this case, the condition on μ_3 must be imposed at the domain outlet, but no information are known a priori to set this value.

It is worth pointing out that the expression for λ_2 in eq.(33) contains also an information related to the mesh, i.e. Δx, and not to the thermodynamics itself.

Furthermore, from the physics of the problem, it is arguably reasonable to impose the liquid phase fraction at the domain inlet, and to extrapolate at the domain outlet the value coming from inside.

C Residual jacobian determination

Eq.(37) can be substituted in eq.(19) obtaining

$$F_{\frac{i+j}{2}} = \frac{F_i + F_j}{2} - \frac{1}{2}\begin{bmatrix} a_2 \cdot U_j(1) \\ b_2 \cdot U_j(1) + c_2 \cdot U_j(2) \end{bmatrix} + \frac{1}{2}\begin{bmatrix} a_2 \cdot U_i(1) \\ b_2 \cdot U_i(1) + c_2 \cdot U_i(2) \end{bmatrix} = \frac{F_i + F_j}{2} - \frac{1}{2}V_j + \frac{1}{2}V_i. \tag{38}$$

Therefore, the flux derivatives are

$$\frac{F_{\frac{i+j}{2}}}{U_i} = \frac{1}{2}\frac{\partial F_i}{\partial U_i} + \frac{1}{2}\frac{\partial F_j}{\partial U_i} - \frac{1}{2}\frac{\partial V_j}{\partial U_i} + \frac{1}{2}\frac{\partial V_i}{\partial U_i}, \tag{39}$$

$$\frac{F_{\frac{i+j}{2}}}{U_j} = \frac{1}{2}\frac{\partial F_i}{\partial U_j} + \frac{1}{2}\frac{\partial F_j}{\partial U_j} - \frac{1}{2}\frac{V_j}{U_j} + \frac{1}{2}\frac{V_i}{U_j}. \tag{40}$$

The physical flux derivative has already been shown in eq.(29), thus

$$\frac{\partial F_i}{\partial U_i}, \frac{\partial F_j}{\partial U_j} = A_i, A_j. \tag{41}$$

Despite of what happens for the conventional single phase, the physical flux F_i depends also on U_j, due to the summatory in eq.(19). Therefore

$$\frac{\partial F_i}{\partial U_j}(1, 1:2) = 0, \tag{42}$$

$$\frac{\partial F_i}{\partial U_j}(2,1) = -\frac{x_i - x_{inlet}}{x_{outlet} - x_{inlet}} \left(G\Delta x \left(\rho_m \mu_0\right)^{-\frac{2}{3}} \left(\rho_m \mu_3\right)^{\frac{2}{3}} \right)_j, \tag{43}$$

$$\frac{\partial F_i}{\partial U_j}(2,2) = -2\frac{x_i - x_{inlet}}{x_{outlet} - x_{inlet}} \left(G\Delta x \left(\rho_m \mu_0\right)^{\frac{1}{3}} \left(\rho_m \mu_3\right)^{-\frac{1}{3}} \right)_j. \tag{44}$$

The last terms in eq.(39) are developed as

$$\frac{\partial V_j}{\partial U_i}(1, 1:2) = 0, \tag{45}$$

$$\frac{\partial V_j}{\partial U_i}(2,1) = U_j(1)\frac{\partial b_2}{\partial U_i(1)} + U_j(2)\frac{\partial c_2}{\partial U_i(1)} \tag{46}$$

$$\frac{\partial V_j}{\partial U_i}(2,2) = U_j(1)\frac{\partial b_2}{\partial U_i(2)} + U_j(2)\frac{\partial c_2}{\partial U_i(2)} \tag{47}$$

and

$$\frac{\partial V_i}{\partial U_i}(1,1) = a_2, \tag{48}$$

$$\frac{\partial V_i}{\partial U_i}(1,2) = 0, \tag{49}$$

$$\frac{\partial V_i}{\partial U_i}(2,1) = U_i(1)\frac{\partial b_2}{\partial U_i(1)} + b_2 + U_i(2)\frac{\partial c_2}{\partial U_i(1)}, \tag{50}$$

$$\frac{\partial V_i}{\partial U_i}(2,2) = U_i(1)\frac{\partial b_2}{\partial U_i(2)} + c_2 + U_i(2)\frac{\partial c_2}{\partial U_i(2)} \tag{51}$$

The same procedure for eq.(40) leads to

$$\frac{\partial V_i}{\partial U_j}(1,1) = 0, \tag{52}$$

$$\frac{\partial V_i}{\partial U_j}(1,2) = 0, \tag{53}$$

$$\frac{\partial V_i}{\partial U_j}(2,1) = U_i(1)\frac{\partial b_2}{\partial U_j(1)} + U_i(2)\frac{\partial c_2}{\partial U_j(1)} \tag{54}$$

$$\frac{\partial V_i}{\partial U_j}(2,2) = U_i(1)\frac{\partial b_2}{\partial U_j(2)} + U_i(2)\frac{\partial c_2}{\partial U_j(2)} \tag{55}$$

and to

$$\frac{\partial V_j}{\partial U_j}(1,1) = a_2, \tag{56}$$

$$\frac{\partial V_j}{\partial U_j}(1,2) = 0, \tag{57}$$

$$\frac{\partial V_j}{\partial U_j}(2,1) = U_j(1)\frac{\partial b_2}{\partial U_j(1)} + b_2 + U_j(2)\frac{\partial c_2}{\partial U_j(1)}, \tag{58}$$

$$\frac{\partial V_j}{\partial U_j}(2,2) = U_j(1)\frac{\partial b_2}{\partial U_j(2)} + c_2 + U_j(2)\frac{\partial c_2}{\partial U_j(2)} \tag{59}$$

Finally, all the quantities a_2, b_2, c_2 are evaluated in

$$U_{\frac{i+j}{2}} = 0.5 \cdot (U_i + U_j), \tag{60}$$

thus, the missing derivatives are

$$\frac{\partial a_2, b_2, c_2}{\partial U_i} = \frac{\partial a_2, b_2, c_2}{\partial U_j} = \frac{\partial a_2, b_2, c_2}{\partial U_{\frac{i+j}{2}}} \cdot \frac{\partial U_{\frac{i+j}{2}}}{\partial U_{i,j}} = \frac{1}{2}\frac{\partial a_2, b_2, c_2}{\partial U_{\frac{i+j}{2}}}, \tag{61}$$

$$\frac{\partial a_2}{\partial U_{\frac{i+j}{2}}} = 0 \tag{62}$$

$$\frac{\partial b_2}{\partial U_{\frac{i+j}{2}}} = \frac{1}{v_m - c_1}\left((v_m - |c_1|)\frac{\partial b_1}{\partial U_{\frac{i+j}{2}}} - b_1\frac{c_1}{\partial U_{\frac{i+j}{2}}}\frac{|c_1|}{c_1}\right) + \frac{b_1\left(v_m - |c_1|\right)}{\left(v_m - c_1\right)^2} \cdot \frac{\partial c_1}{\partial U_{\frac{i+j}{2}}}, \tag{63}$$

$$\frac{\partial c_2}{\partial U_{\frac{i+j}{2}}} = \frac{\partial c_1}{\partial U_{\frac{i+j}{2}}}\frac{|c_1|}{c_1}, \tag{64}$$

in which

$$\frac{\partial b_1}{\partial U_{\frac{i+j}{2}}(1)} = \frac{2}{3}\left(\frac{x - x_{inlet}}{x_{outlet} - x_{inlet}} G\Delta x \left(\rho_m \mu_0\right)^{-\frac{5}{3}} \left(\rho_m \mu_3\right)^{\frac{2}{3}}\right)_{\frac{i+j}{2}}, \tag{65}$$

$$\frac{\partial b_1}{\partial U_{\frac{i+j}{2}}(2)} = -\frac{2}{3}\left(\frac{x - x_{inlet}}{x_{outlet} - x_{inlet}} G\Delta x \left(\rho_m \mu_0\right)^{-\frac{2}{3}} \left(\rho_m \mu_3\right)^{-\frac{1}{3}}\right)_{\frac{i+j}{2}}, \tag{66}$$

$$\frac{\partial c_1}{\partial U_{\frac{i+j}{2}}(1)} = -\frac{2}{3}\left(\frac{x - x_{inlet}}{x_{outlet} - x_{inlet}} G\Delta x \left(\rho_m \mu_0\right)^{-\frac{2}{3}} \left(\rho_m \mu_3\right)^{-\frac{1}{3}}\right)_{\frac{i+j}{2}}, \tag{67}$$

$$\frac{\partial c_1}{\partial U_{\frac{i+j}{2}}(2)} = -\frac{2}{3}\left(\frac{x - x_{inlet}}{x_{outlet} - x_{inlet}} G\Delta x \left(\rho_m \mu_0\right)^{\frac{1}{3}} \left(\rho_m \mu_3\right)^{-\frac{4}{3}}\right)_{\frac{i+j}{2}}. \tag{68}$$

D Nozzle geometry

The nozzle area A_c is given by

$$A_c(x) = \begin{cases} a_0 + b_0 x + c_0 x^2 + d_0 x^3 & 0.0 < x < 0.041837 \\ a_1 + b_1 x + c_1 x^2 + d_1 x^3 & 0.041837 < x < 0.10612 \\ a_2 + b_2 x + c_2 x^2 + d_2 x^3 & 0.10612 < x < 0.4 \end{cases}, \tag{69}$$

in which x is expressed in m and A_c in m^2. All the missing coefficient are reported in the table below [7] .

	a	b	c	d
0	$1.52{\cdot}10^{-2}$	$-5.1996{\cdot}10^{-4}$	$6.7416{\cdot}10^{-1}$	-8.7727
1	$1.533{\cdot}10^{-2}$	$8.0338{\cdot}10^{-3}$	$2.6189{\cdot}10^{-2}$	$7.3488{\cdot}10^{-3}$
2	$1.4926{\cdot}10^{-2}$	$1.4733{\cdot}10^{-2}$	$5.4451{\cdot}10^{-5}$	$-2.0589{\cdot}10^{-4}$

Table 3: Nozzle profile coefficients